Separation Science and Technology
Publication details, including instructions for authors and subscription information:
http://www.informaworld.com/smpp/title~content=t713708471

Column Dynamics for Adsorption of Bulk Binary Gas Mixtures on Activated Carbon

S. Sircar[a]; R. Kumar[a]
[a] Air Products and Chemicals, Inc., Allentown, Pennsylvania

To cite this Article Sircar, S. and Kumar, R.(1986) 'Column Dynamics for Adsorption of Bulk Binary Gas Mixtures on Activated Carbon', Separation Science and Technology, 21: 9, 919 — 939
To link to this Article: DOI: 10.1080/01496398608058387
URL: http://dx.doi.org/10.1080/01496398608058387

SEPARATION SCIENCE AND TECHNOLOGY, 21(9), pp. 919-939, 1986

Column Dynamics for Adsorption of Bulk Binary Gas Mixtures on Activated Carbon

S. SIRCAR* and R. KUMAR

AIR PRODUCTS AND CHEMICALS, INC.
ALLENTOWN, PENNSYLVANIA 18105

Abstract

Dynamics of adsorption from bulk N_2-He, CH_4-He, CO_2-He, CO_2-N_2, and CO_2-CH_4 binary mixtures were measured in a column packed with the BPL activated carbon. The data were analyzed using an adiabatic, isobaric, constant pattern model of column adsorption in conjunction with a linear driving force model for the adsorbate mass transfer. It was found that the mass transfer coefficients for adsorption of CO_2, CH_4, and N_2 were significantly lower during binary co-adsorption in the presence of each other than the corresponding pure component mass transfer coefficients in the presence of nonadsorbing helium. The reduction was more pronounced for the less strongly adsorbed species of the binary mixture. This kinetic interaction between the adsorbates could not be predicted *a priori*. Equilibrium isotherms for adsorption of pure N_2, CH_4, and CO_2 and for adsorption of CO_2-N_2 and CO_2-CH_4 binaries were also measured on the carbon. The isotherms obeyed the Langmuir equation.

The dynamics of adsorption of a gas mixture in a packed adsorbent column is governed by the competitive adsorption equilibria and the interactive gas to solid mass transfer between the components of the mixture. The multicomponent adsorption equilibria at the column conditions may be estimated from the pure gas equilibrium adsorption characteristics of the components using many published theories (*1, 2*). The interactive mass transfer of the components, on the other hand, is much less studied and cannot generally be predicted from the pure component adsorption kinetics data.

The adsorbate mass transfer may be controlled by the gas film

*To whom correspondence should be addressed.

 0149-6395/86/2109-0919$3.50/0

resistance outside the adsorbent particle, the internal macro- and micropore gas diffusional resistances, the resistance to surface diffusion of the adsorbed molecules within the adsorbent, or combination of these resistances. Many correlations exist to calculate the external gas film resistances (*3, 4*). Models of porous solids have been formulated to estimate the steady-state pore diffusion of multicomponent gas mixtures across them (*4–6*). Models are also proposed to evaluate the surface diffusivity of a single adsorbate on a homogeneous adsorbent (*7, 8*). However, these models can only provide an order of magnitude estimation of the mass transfer coefficients for the adsorbates of a mixture. They should be used with caution because the pore structures of most practical adsorbents are very complex and the adsorbent surface is generally heterogeneous.

A simplified design practice is to assume that the adsorbate mass transfer is noninteractive. The assumption has been found to be valid for several cases of isothermal adsorption of two dilute adsorbates from an inert carrier gas (*9–11*). The purpose of this work is to investigate the mass transfer interactions between the components of a bulk binary gas mixture during nonisothermal adsorption in an adiabatic column.

EXPERIMENTAL TESTS AND RESULTS

A granular BPL activated carbon (6–16 mesh) produced by the Calgon Corporation was used as the adsorbent. The diameter of the adsorbent particles varied between 0.06 to 0.31 cm with a Sauter mean diameter (d_p) of 0.215 cm. The bulk (ρ_b) and the particle (ρ_p) densities of the carbon were, respectively, 0.498 and 0.872 g/cm^3. The carbon was dried at ~120°C under vacuum or using a dry helium purge before the experiments. The adsorbates were carbon dioxide, methane, and nitrogen.

Pure gas adsorption isotherms for CO_2, CH_4, and N_2 were measured at ~30 and 69°C in the pressure range of 0–2 atm using a volumetric adsorption apparatus. Figures 1–3 show the experimental pure gas isotherms (circles). The binary adsorption isotherms for CO_2–CH_4 and CO_2–N_2 mixtures were measured at 31°C and atmospheric pressure using a desorption technique described elsewhere (*12*). Figures 4 and 5 show the experimental binary isotherms (circles).

The column dynamics for adsorption of the pure gases were measured by flowing a ~25% mixture of the adsorbates (CO_2, CH_4, and N_2) in a nonadsorbing carrier gas (helium) through an externally insulated packed adsorbent column (2″ diameter × 48″ long) at near ambient pressure and temperature and monitoring the adsorbate concentration in

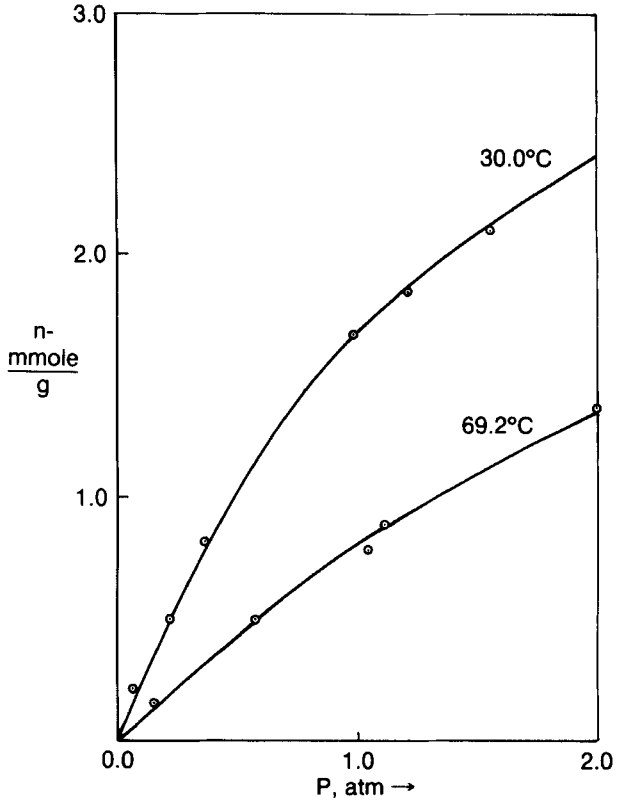

FIG. 1. Isotherms for adsorption of CO_2 on BPL carbon: (O) experiment, (—) theory.

the effluent gas as a function of time. The central line column temperature at the effluent end of the column and the quantity of the effluent gas were also measured as functions of time using a shielded 1/16 in. thermocouple and a dry test meter. The column was initially free of the adsorbates and saturated with pure helium at the feed gas pressure and temperature. The feed gas flow rates and the other test conditions are given in Table 1. The effluent gas analysis was carried out using an infrared analyzer, a hydrocarbon analyzer, and a thermal conductivity detector for the adsorbates CO_2, CH_4, and N_2, respectively. Figures 6(a–c), respectively, show the experimental (circles) adsorbate breakthrough curves for adsorption of ~25.0% N_2, CH_4, and CO_2 from helium. Figure 7 shows a typical experimental (crosses) adsorbent temperature-time

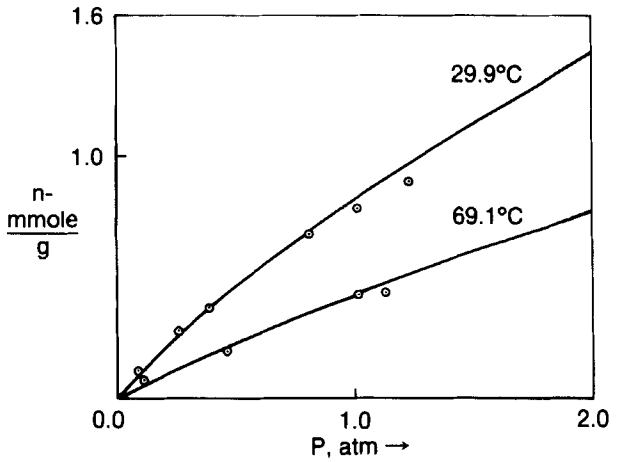

FIG. 2. Isotherms for adsorption of CH_4 on BPL carbon: (O) experiment, (—) theory.

profile at the effluent end of the column for the CO_2-He breakthrough run.

The column dynamics for adsorption of the binary gas mixtures were measured in another externally insulated column (2″ diameter × 96″ long) with sample taps at 24, 48, 72, and 96 in. from the feed end. The feed gas comprised a ~25% mixture of CO_2 in CH_4 or N_2 which was passed through the column at near ambient pressure and temperature. The column was initially saturated with pure CH_4 or N_2 at the feed gas conditions. The gas compositions and the central line adsorbent temperatures were measured as functions of time at all four sample taps.

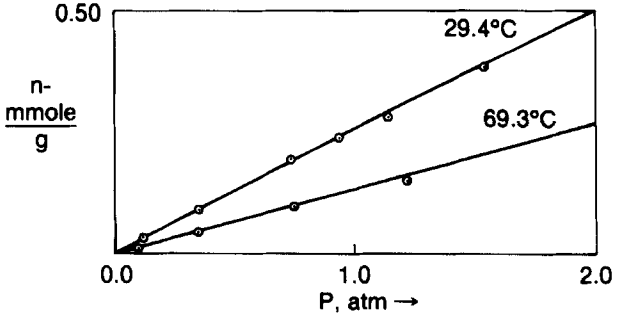

FIG. 3. Isotherms for adsorption of N_2 on BPL carbon: (O) experiment, (—) theory.

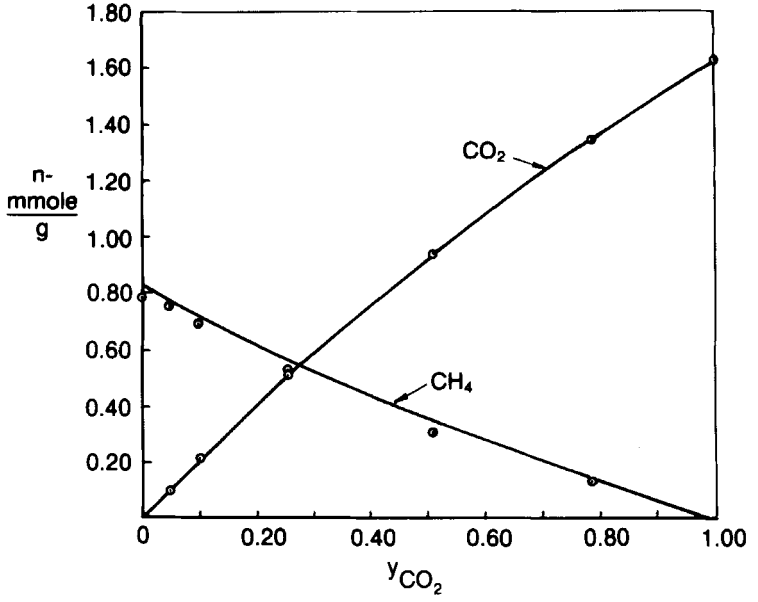

FIG. 4. Binary adsorption isotherms for CO_2-CH_4 mixtures on BPL carbon at $P = 1.0$ atm, $T = 31°C$: (O) experiment, (—) theory.

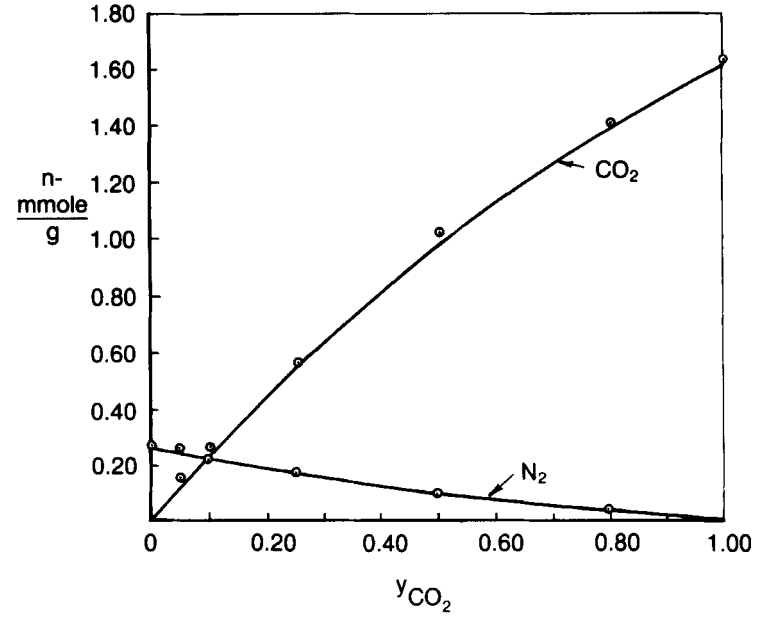

FIG. 5. Binary adsorption isotherms for CO_2-N_2 mixtures on BPL carbon at $P = 1.0$ atm, $T = 31°C$: (O) experiment, (—) theory.

TABLE 1
Dynamic Test Conditions and Properties of the Front MTZ

Systems	Q°	Q^*	Q^s	β	y_1°	y_1^*	θ* (°C)		T°	P
	mmol/cm²/s			(cm/s)			Expt.	Theory	(°C)	(atm)
$N_2(1)$ + He(2)	1.15	1.15	0.92	5.6	0.251	0.251	2.4	1.7	22	1.35
$CH_4(1)$ + He(2)	1.32	1.32	1.02	2.6	0.251	0.248	9.2	6.5	22	1.31
$CO_2(1)$ + He(2)	2.09	2.08	1.59	2.1	0.251	0.247	16.5	15.5	22	1.30
$CO_2(1)$ + $N_2(2)$	2.09	2.08	1.72	1.7	0.253	0.250	13.7	12.2	22	1.20
$CO_2(1)$ + $CH_4(2)$	1.89	1.88	1.77	1.5	0.245	0.244	7.2	6.6	22	1.20

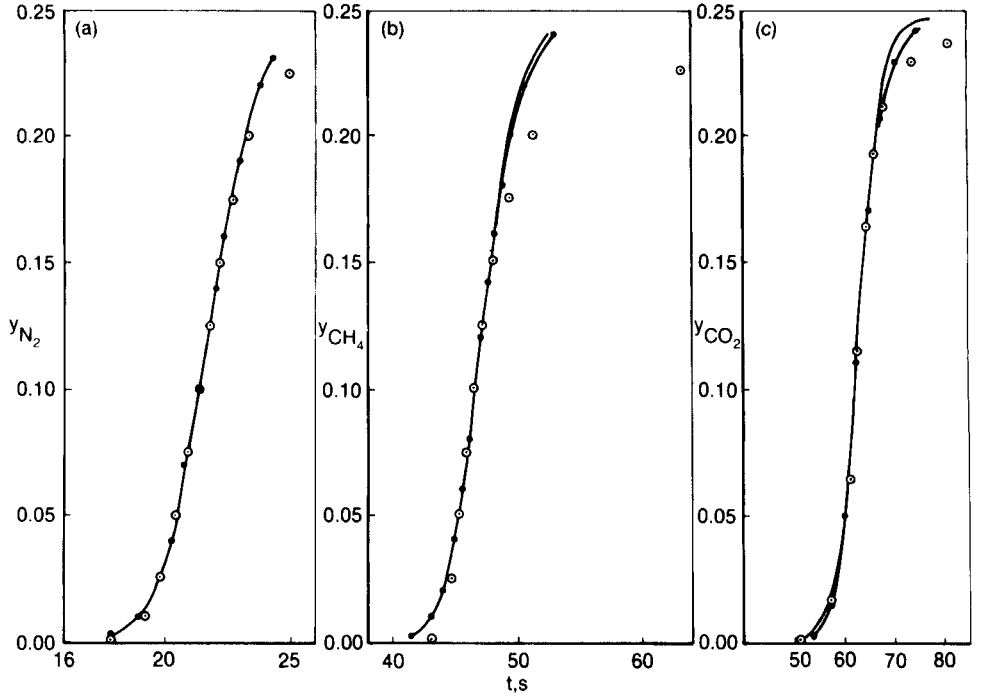

FIG. 6. Breakthrough curves for adsorption of (a) N_2, (b) CH_4, and (c) CO_2 from helium on BPL carbon at a column length of 48 in.: (○) experiment, (—) Eq. 4(a), (- -) Eq. 4(b).

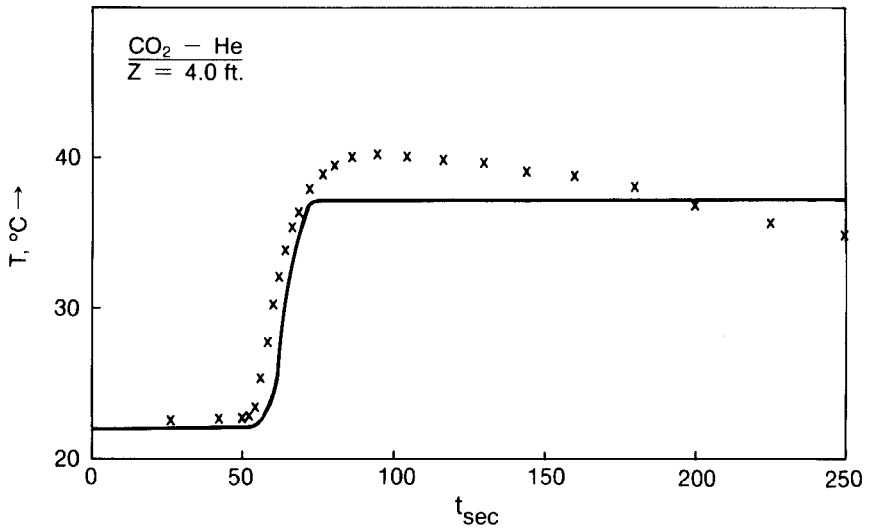

FIG. 7. Adsorbent temperature-time profile for adsorption of CO_2–He mixture at a column length of 48 in.: (×) experiment, (—) Eq. 4(a).

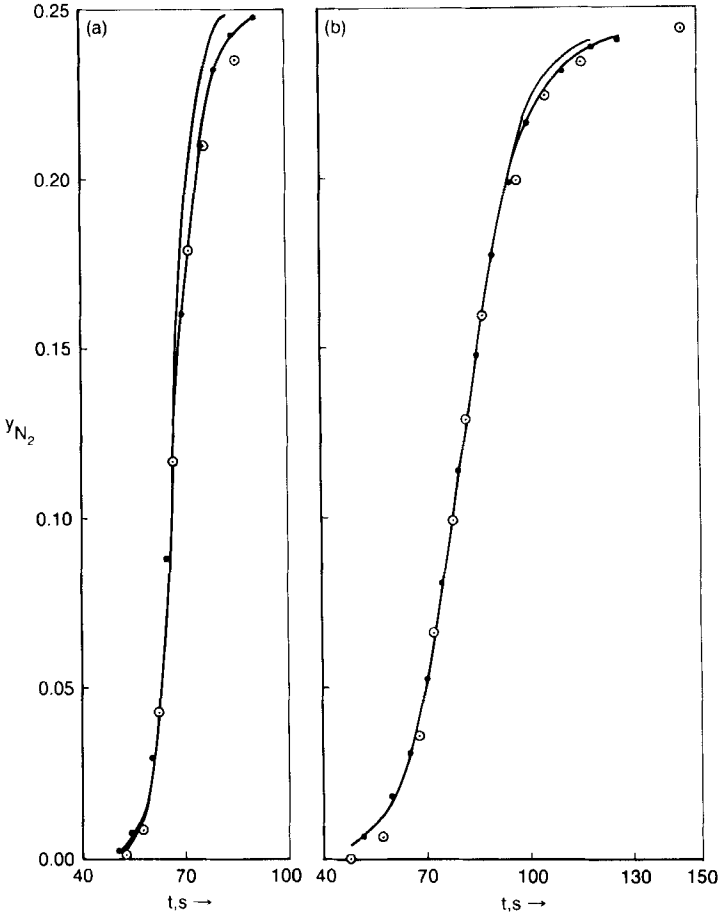

FIG. 8. CO_2 breakthrough curves for adsorption of (a) CO_2-CH_4 and (b) CO_2-N_2 binary mixtures on BPL carbon at a column length of 48 in.: (O) experiment, (—) Eq. 4(a), (- -) Eq. 4(b).

The column effluent gas quantity was also measured as a function of time. The CO_2 infrared analyzer was employed to measure the gas concentrations. Table 1 reports the test conditions. Figures 8(a) and 8(b), respectively, show the experimental (circles) CO_2 breakthrough curves at a column height of 48 in. from the feed end for adsorption of CO_2-CH_4 and CO_2-N_2 mixtures. Figure 9 shows the corresponding experimental (crosses) adsorbent temperature-time profiles for the CO_2-CH_4 adsorption system.

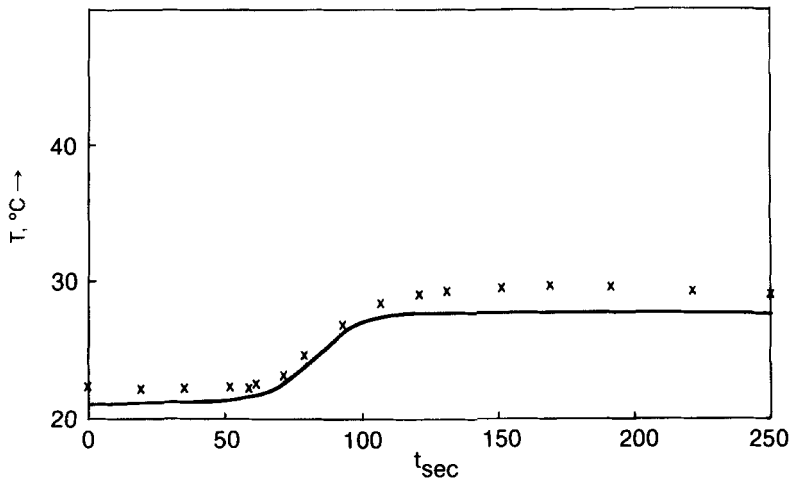

FIG. 9. Adsorbent temperature-time profiles for adsorption of CO_2-CH_4 mixtures at a column length of 48 in.: (×) experiment, (—) Eq. 4(a).

ANALYSIS OF THE DATA

Equilibrium Adsorption

The pure gas isotherms for adsorption of CO_2, CH_4, and N_2 on the carbon could be described in the P and T ranges of this work by the Langmuir model:

$$\hat{n}_i = \frac{m\hat{b}_i P}{1 + \hat{b}_i P} \tag{1}$$

$$\hat{b}_i = \hat{C}_i e^{q_i/RT} \tag{2}$$

The variables are defined in the nomenclature.

The solid lines in Figs. 1-3 describe the best fit of the pure gas isotherms using the Langmuir parameters (m, $\hat{C}_i$, and q_i) summarized in Table 2. Since the same value of m could be used to describe the pure gas isotherms for all three gases, the mixed Langmuir model (*1*) was used to calculate the binary gas adsorption isotherms for a given P, T, and y_i:

TABLE 2
Pure Gas Langmuir Parameters

	m (mmol/g)	$\hat{C}_i$ (atm^{-1})	q_i (kcal/mol)
CO_2	4.35	9.45×10^{-5}	5.29
CH_4	4.35	23.6×10^{-5}	4.17
N_2	4.35	24.7×10^{-5}	3.34

$$\bar{n}_i = \frac{m\hat{b}_i P y_i}{1 + \sum \hat{b}_i P y_i} \tag{3}$$

The solid lines in Figs. 4 and 5, respectively, show the $\bar{n}_i$ against y_i plots for adsorption of the CO_2-CH_4 and the CO_2-N_2 binary mixtures on the carbon at 31°C and a total gas pressure of 1 atm calculated by using Eq. (3) and the pure component Langmuir parameters of Table 2. The figures show that Eq. (3) can very well describe the binary isotherms for these systems at the conditions of interest.

The isosteric heats of adsorption for the adsorbates decreased in the order $CO_2 > CH_4 > N_2$, indicating that the strengths of adsorption of these gases on the carbon also decreased in the same order. The binary selectivity of adsorption ($S_{12} = \hat{b}_1/\hat{b}_2$) of CO_2 (Component 1) from CH_4 and N_2 (Component 2) at 30°C were, respectively, 2.3 and 9.8. Thus the coadsorption of CH_4 and N_2 on the carbons in presence of CO_2 differed significantly, and these binary mixtures provided interesting cases for the study of interactive mass transfers between the components.

Column Dynamics

The column dynamics for adsorption of bulk CO_2, CH_4, and N_2 from helium and those for CO_2-CH_4 and CO_2-N_2 binary mixtures on the carbon exhibited Type I characteristics (*13, 14*) at the test conditions of this study. Two pairs of mass and heat transfer zones were formed in the column separated by an equilibrium section described by [Q^*, y_i^*, T^*, and $\bar{n}_i^*$]. The column ahead of the front transfer zone was under equilibrium at the initial column conditions [Q^s, y_i^s, T^s, and $\bar{n}_i^s$] and the column behind the rear transfer zones was equilibrated at the feed gas conditions [Q°, y_i°, T°, and $\bar{n}_i^\circ$].

The adsorbate breakthrough data and the column temperature-time

profiles given by Figs. 6–9 are for the front pair of the mass and heat transfer zones. It was found that the front transfer zones for these systems were constant pattern. The lengths (L_m) of the mass transfer zones (MTZ) did not change after the zones traveled through a distance of 24 in. from the feed end. For example, L_m bounded by a CO_2 mole fraction of 0.01 to 0.24 for adsorption of the CO_2–CH_4 mixture were, respectively, 19, 22.6, and 21.6 in. at column heights of 48, 72, and 96 in.

The adiabatic, isobaric, constant pattern (AICP) model for adsorption of a bulk single or bulk binary gas mixture [13] was then used to analyze the column dynamics for these systems and to evaluate the overall adsorptive mass transfer coefficient for the adsorbates. The model provided explicit relationship between y_i, n_i, T, and Q at various points in the front transfer zones. It also furnished the values of the parameters Q^*, Q^s, T^*, y_i^*, and the velocity (β) of the front zone. They are reported in Table 1. It was assumed that the local rate of adsorption of the components in the front transfer zone were given by the linear driving force (LDF) models with constant overall mass transfer coefficients ($k^\circ_{n_i}$ or $k^\circ_{y_i}$) for the adsorbates:

$$\left(\frac{\partial n_i}{\partial t}\right)_z = k^\circ_{n_i}[\bar{n}_i - n_i] \tag{4a}$$

$$= k^\circ_{y_i}[y_i - \bar{y}_i] \tag{4b}$$

Equations (4a) and (4b) represent two different driving forces (adsorbate loading or concentration difference) for the rate process. $\bar{n}_i$ is related to y_i by Eq. (3). $\bar{y}_i$ is related to n_i by

$$n_i = \frac{m\hat{b}_i P\bar{y}_i}{1 + \sum \hat{b}_i P\bar{y}_i} \tag{5}$$

Equations (4a) and (4b) can be integrated to obtain the time difference $\tau_z(y_i)$ during which the concentration of the front MTZ changes between y_i^s to y_i or the adsorbate loading changes between n_i^s and n_i at any distance z in the column:

$$\tau_z(y_i) = \frac{1}{k^\circ_{n_i}} \int_{n_i^s}^{n_i} \frac{dn_i}{(\bar{n}_i - n_i)} \tag{6a}$$

$$= \frac{1}{k^\circ_{y_i}} \int_{y_i^s}^{y_i} \frac{dn_i}{(y_i - \bar{y}_i)} \tag{6b}$$

The integrals of Eqs. (6a) and (6b) can be numerically evaluated using the relationship between n_i, y_i, and T in the front transfer zone provided by the solution of the AICP model and the equilibrium isotherms given by Eqs. (3) and (5). The values of these integrals at different y_i can then be plotted against the corresponding $\tau_z(y_i)$ values from the experimental breakthrough curves at a distance z in the column. These plots, according to Eqs. (6a) or (6b), should be straight lines with slopes equal to $k^\circ_{n_i}$ or $k^\circ_{y_i}$. Thus the overall mass transfer coefficients for the adsorbates can be estimated from the dynamic adsorption data. Figures 10(a) and 10(b), respectively, show examples of the above-described plots for adsorption of ~25% N_2 from helium and for adsorption of 25% CO_2 from CH_4. The breakthrough data of Component 1 at a column height of 48 in. from the feed end was used in these figures in conjunction with Eqs. (4a) and (6a). It may be seen that the plots are fairly linear for the entire length of the front MTZ except in the region of $y_1 \rightarrow y_1^*$ (trailing edge of the front MTZ). This deviation from linearity can be explained in terms of the column nonadiabaticity which stretches the trailing edge of the front MTZ (*15*) due to cooling of the middle equilibrium section of the Type I system. Figure 7 provides evidence of this cooling phenomenon by the slow drop of the column central line temperature. The adsorbent near the column wall undergoes a larger drop in the temperature. Consequently, the plots of Figs 10(a) and 10(b) become more nonlinear in the high y_1 region as the zones propagate farther through the column.

A similar procedure was used to calculate $k^\circ_{n_2}$ for the less strongly adsorbed species of the mixtures of this study. In addition, Eqs. (4b) and (6b) were used to obtain $k^\circ_{y_i}$ for the adsorbates using an analogous analysis. Table 3 reports these overall mass transfer coefficients.

The recalculated concentration breakthrough curves using these mass transfer coefficients, the equilibrium isotherms, the solutions of the AICP model, and Eqs. (6a) and (6b) are shown by the solid lines in Figs. 6 and 8. They show that the AICP model with the LDF mass transfer mechanism can very well describe the column dynamics for the systems of this study except in the trailing edge of the MTZs due to reasons discussed earlier. The solid lines in Figs. 7 and 9 show the model calculations of the adsorbent temperature-time profiles for the appropriate systems. Again the match between the theory and the experiment is very good. An important conclusion from these analyses is that the breakthrough data for all systems studied in this work can be described equally well by either of the LDF mechanisms of Eqs. (4a) and (4b) by using a constant mass transfer coefficient for the adsorbates.

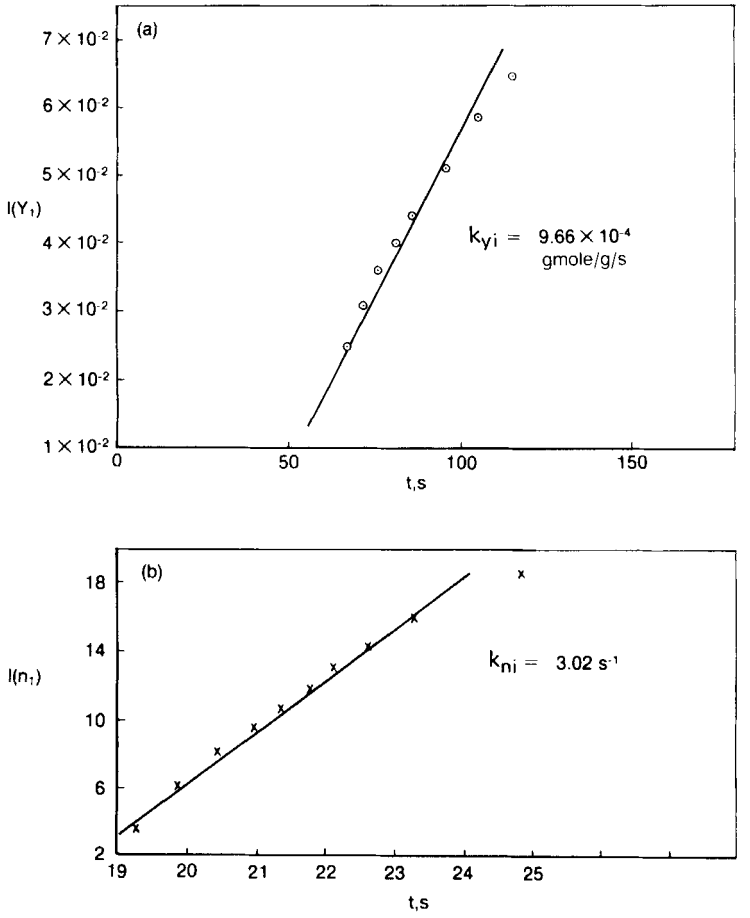

FIG. 10. Plots of Eqs. (6a) and (6b) for adsorption of (a) N_2-He and (b) CO_2-CH_4 mixtures on BPL carbon.

TABLE 3
Mass Transfer Coefficients, Pore and Surface Diffusivities

Systems	$\bar{T}$ (°C)	k_f	$k^\circ_{y_1}$	$k^\circ_{y_2}$	$k^\circ_{n_1}$	$k^\circ_{n_2}$	$k^a_{n_1}$	$k^a_{n_2}$	$\tilde{D}_{p_1}$	$\tilde{D}_{p_2}$	$k^a_{p_1}$	$k^a_{p_2}$
		mmol/g/s			s^{-1}		s^{-1}		$cm^2/s \times 10^2$		s^{-1}	
$N_2(1)$ + He(2)	22.8	13.0	1.30	—	3.020	—	3.33	—	1.73	5.21	3.57	—
$CH_4(1)$ + He(2)	25.3	16.3	1.89	—	1.282	—	1.42	—	1.94	6.81	1.13	—
$CO_2(1)$ + He(2)	29.7	17.4	1.34	—	0.413	—	0.44	—	1.57	7.21	0.42	—
$CO_2(1)$ + $N_2(2)$	28.1	11.9	1.15	0.30	0.322	0.704	0.35	0.76	0.61	1.22	0.16	2.00
$CO_2(1)$ + $CH_4(2)$	25.3	14.5	0.94	0.90	0.335	0.614	0.35	0.66	0.59	0.79	0.17	0.44

External Film and Internal Mass Transfer Resistances

The external film mass transfer coefficient (k_f) in the front MTZ varies across the zone length due to variation of Q, y_i, and T in the zone. We estimated an average $\tilde{k}_f$ for the MTZ using the average values of these variables $\tilde{Q}[= (Q^s + Q^*)/2]$, $\tilde{y}_i[= (y_i^s + y_i^*)/2]$, and $\tilde{T}[= (T^s + T^*)/2]$ in the zone and the following correlation (*16*):

$$\tilde{k}_f = \frac{2.88\tilde{Q}}{\varepsilon \rho_p d_p} (\tilde{\mathrm{Re}})^{-0.39} (\tilde{\mathrm{Sc}})^{0.67} \tag{7}$$

Table 3 summarizes the $\tilde{k}_f$ values.

The adsorbate mass transfer in a constant pattern transfer zone may be treated as a pseudosteady-state process because the zone does not change its shape as it moves through the column with a constant velocity. Consequently, we define an average rate of adsorption ($\tilde{N}_i$) for the component i of the mixture per unit amount of the adsorbent in the front MTZ of the Type I system. A mass balance across the front MTZ gives

$$\tilde{N}_i = [Q^* y_i^* - Q^s y_i^s]/L_m \rho_b \tag{8a}$$

$$\tilde{N} = \sum \tilde{N}_i = [Q^* - Q^s]/L_m \rho_b \tag{8b}$$

$L_m[= \beta \tau_z(y_i^*)]$ is the length of the front MTZ. Equations (8a) and (8b) can be used to calculate $\tilde{N}_i$ and $\tilde{N}$ using the solutions of the AICP model.

$\tilde{N}_i$ may also be written as

$$\tilde{N}_i = \tilde{k}_f[\tilde{y}_i - \tilde{y}_{f_i}] + \tilde{y}_i[\tilde{N}] \tag{9a}$$

$$= k_{n_i}^{\circ}[\tilde{\bar{n}}_i - \tilde{n}_i] \tag{9b}$$

$$= k_{n_i}^{a}[\tilde{\bar{n}}_{f_i} - \tilde{n}_i] \tag{9c}$$

Equations (9a–c) describe $\tilde{N}_i$ in terms of the average properties of the MTZ.

$\tilde{y}_{f_i}$ can be obtained from Eq. (9a):

$$\tilde{y}_{f_i} = \tilde{y}_i - \frac{\tilde{N}_i - \tilde{y}_i \tilde{N}}{\tilde{k}_f} \tag{10}$$

$\tilde{\bar{n}}_{f_i}$ and $\tilde{\bar{n}}_i$ can then be calculated using Eq. (3) at P and $\tilde{T}$ by replacing y_i with, respectively, $\tilde{y}_{f_i}$ and $\tilde{y}_i$. The internal mass transfer coefficient of the

adsorbent particle ($k^a_{n_i}$) for Component i is then obtained from Eqs. (9b) and (9c) as

$$\frac{1}{k^a_{n_i}} = \frac{1}{k^\circ_{n_i}} - \frac{\tilde{\bar{n}}_i - \tilde{\bar{n}}_{f_i}}{\tilde{N}_i} \tag{11}$$

Table 3 reports the $k^a_{n_i}$ values for the systems studied. The differences between $k^\circ_{n_i}$ and $k^a_{n_i}$ indicate that the external film mass transfer resistances ranged between ~10–20% of the overall mass transfer reistance for these systems.

Internal Mass Transfer Resistances

It may be seen from Table 3 that the overall internal mass transfer coefficients ($k^a_{n_i}$) for adsorption of CO_2, CH_4, and N_2 in the presence of nonadsorbing He on the BPL carbon is significantly higher than the mass transfer coefficients for these gases when adsorbing with a coadsorbing species. For example, $k^a_{n_i}$ for CO_2 in the presence of He is 0.44 s^{-1}, which decreases to 0.35 s^{-1} when adsorbing in the presence of CH_4 or N_2. The $k^a_{n_i}$ for CH_4 in the presence of He is 1.42 s^{-1}, which decreases to 0.66 s^{-1} in the presence of CO_2. The effect is largest for N_2 which has $k^a_{n_i}$ values of, respectively, 3.33 and 0.76 s^{-1} in the presence of He and CO_2. These results show that the mass transfer coefficients of a bulk adsorbing gas can be significantly affected (reduced) by the presence of a coadsorbing species. The reduction is more pronounced for the less strongly adsorbed species of the mixture. Furthermore, N_2 competes far less strongly with CO_2 than CH_4 for adsorption on the carbon, and thus it undergoes a much larger reduction in the $k^a_{n_i}$ value than that for CH_4 in the presence of CO_2. It should be pointed out that $k^\circ_{n_i}$ or $k^\circ_{y_i}$ were assumed to be constants in the above analysis. In general, the mass transfer coefficients can be functions of the adsorbent temperature. The average MTZ temperatures ($\tilde{T}$) for the experimental runs reported in this work were not identical. However, that does not alter the conclusion reached above. For example, $\tilde{T}$ for the N_2–He run was ~6°C lower than that for the CO_2–N_2 run. Thus, $k^a_{n_i}$ for N_2 should be larger for the latter case due to higher adsorbent temperature if adsorbate interaction during mass transfer was absent.

It may be concluded that a significant mass transfer interaction between the components of a bulk gas mixture can occur during the adsorption process, and the assumption of a noninteracting mass transfer phenomenon can lead to erroneous process design. It will be demon-

strated in the following section that *a priori* prediction of the mass transfer interactions may not be possible.

Analysis of the Internal Resistances

The overall internal mass transfer coefficient ($k^a_{n_i} = k^a_{p_i} + k^a_{s_i}$) can be written as a summation of the pore diffusion ($k^a_{p_i}$) and the surface diffusion ($k^a_{s_i}$) contributions (*3*):

$$k^a_{p_i} = \frac{\tilde{\Psi}_{p_i} 60 \tilde{D}_{p_i}(1 - \varepsilon)}{\tilde{\Lambda}_i dp^2} \tag{12a}$$

$$k^a_{s_i} = \frac{\tilde{\Psi}_{s_i} 60 \tilde{D}_{s_i}}{dp^2} \tag{12b}$$

Equations (12a) and (12b) are applicable for the LDF mechanism of mass transfer according to Eq. (9c) under constant pattern zone formation (*3*). The parameters $\tilde{\Psi}_{s_i}$, $\tilde{\Psi}_{p_i}$, and $\tilde{\Lambda}_i$ are defined in the nomenclature. We first estimated the pore diffusion contributions to the mass transfer reistances for the systems studied. The adsorbent pore diffusivities ($\tilde{D}_{p_i}$) for the adsorbate i of each system were calculated using the random pore distribution model for bidispersed pores (*5, 6*) and the mean properties of the zones:

$$\tilde{D}_{p_i} = \tilde{D}\left[\frac{\varepsilon_l^2}{(1 - \alpha\tilde{y}_i) + \tilde{D}/\tilde{D}^l_{k_i}} + \frac{\varepsilon_s^2}{(1 - \alpha\tilde{y}_i) + \tilde{D}/\tilde{D}^s_{k_i}} + \frac{4\varepsilon_l(1 - \varepsilon_l)}{(1 - \alpha\tilde{y}_i)\left\{1 + \frac{(1 - \varepsilon_l)^2}{\varepsilon_s^2}\right\} + \frac{\tilde{D}}{\tilde{D}^s_{k_i}}\left\{\frac{(1 - \varepsilon_l^2)}{\varepsilon_s^2} + \frac{\tilde{D}^s_{k_i}}{D^l_{k_i}}\right\}}\right] \tag{13}$$

The BPL carbon had a bimodal pore distribution as shown by the mercury porosimetry data in Fig. 11. The mean pore diameters of the small and the large pore regions were 30 Å and 1.37 μm with pore void fractions of, respectively, 0.396 (ε_s) and 0.189 (ε_p). The bulk gas diffusivity ($\tilde{D}$) for the mixtures were calculated using the Chapman-Enskog model (*4*). The values of $\tilde{D}_{p_i}$ are reported in Table 3 which also gives the calculated $k^a_{p_i}$ values using Eq. (12a).

It may be seen from Table 3 that the calculated $k^a_{p_i}$ values for adsorption of CO_2 and N_2 from He on the carbon are very close to the corresponding $k^a_{n_i}$ values while the $k^a_{p_i}$ for the CH_4-He system is ~25% smaller than the

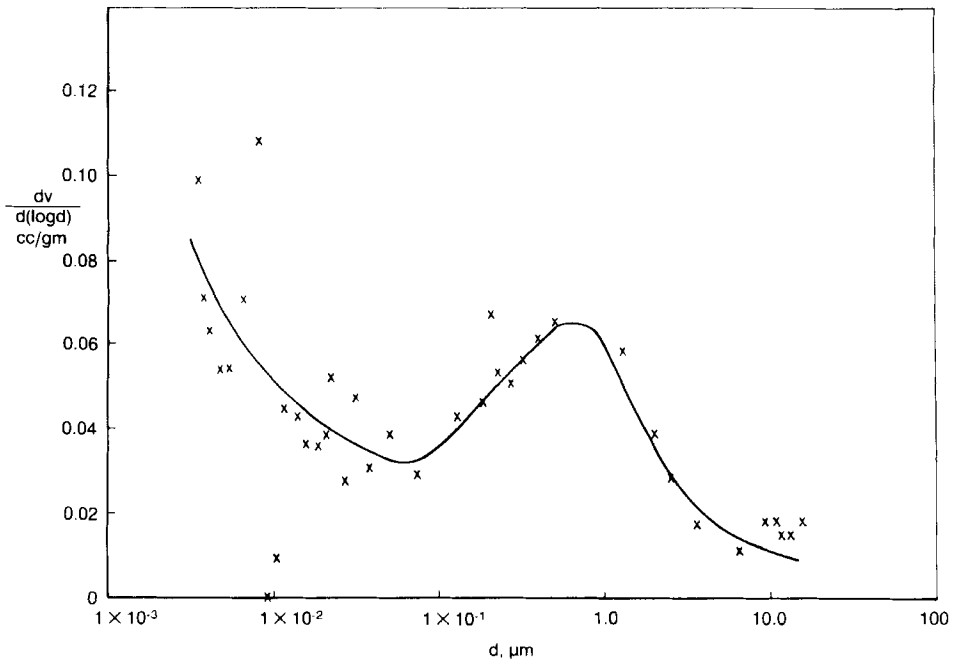

FIG. 11. Pore size distribution of BPL carbon.

experimentally estimated $k_{n_i}^a$ value for that system. Thus it appears that the mass transfer for adsorption of CO_2, CH_4, and N_2 into the carbon in the absence of a competing species is essentially pore diffusion controlled. Thus it is expected that Eqs. (12a) and (13) can be used to calculate the interactive mass transfer coefficients for the binary CO_2–CH_4 and CO_2–N_2 systems. However, Table 3 shows that such calculations underestimate the $k_{n_i}^a$ values for CO_2 by approximately a factor of 2 while the $k_{n_i}^a$ values are severely underpredicted for adsorption of CH_4 and overpredicted for adsorption of N_2 in the presence of CO_2. This indicates that the true mechanism of adsorption kinetics may not be ascertained unequivocally by the analysis of the column breakthrough data, and simple models like Eqs. (12) and (13) may only give an order of magnitude of the mass transfer resistances. Furthermore, the interactive mass transfer between the different adsorbate species of a gas mixture may be very complex and unpredictable. Actual batch kinetic data or column breakthrough data for the gas mixtures of interest may be needed for evaluation and understanding of the kinetic interactions.

It should also be emphasized that the common practice of estimating the extent of surface diffusion for an adsorbate by the difference between the total internal mass transfer resistance and the calculated pore diffusion resistance may be questionable due to the uncertainties in evaluating the latter resistance by a model.

CONCLUSIONS

The column dynamics for adsorption of bulk binary mixtures of N_2, CH_4, and CO_2 in helium and for adsorption of binary $CO_2 + CH_4$ and $CO_2 + N_2$ mixtures on the BPL activated carbon can be described very well using the adiabatic, isobaric, constant pattern model for column adsorption and linear driving force models for mass transfer. The driving forces represented by either Eq. (4a) or Eq. (4b) can be used. It is found that the mass transfer coefficient of an adsorbate can be significantly reduced by the presence of a competing adsorbate in the system compared to its mass transfer coefficient for adsorption in the presence of a nonadsorbable gas. The effect is more pronounced when the adsorbate is weakly adsorbed on the solid. It may not be possible to determine the mechanism of adsorption unequivocally from the analysis of the column breakthrough data. Simple available theories for calculating mass transfer coefficients may only provide an order of magnitude calculation of this property.

SYMBOLS

A_i $(\tilde{y}_i - y_i^s)(n_i^* - \tilde{n}_i)/(\tilde{n}_i - n_i^s)(y_i^* - \tilde{y}_i)$

$\hat{b}$ Langmuir parameter, Eq. (1)

$\hat{C}$ Langmuir parameter, Eq. (2)

dp mean adsorbent particle diameter

D_p pore diffusivity

D_s surface diffusivity

D_k Knudsen diffusivity

D molecular diffusivity

k_f external film mass transfer coefficient, Eq. (7)

$k_{y_i}^o$ overall mass transfer coefficient for Component i, Eq. (4b)

$k_{n_i}^a$ overall internal mass transfer coefficient for Component i based on Eq. (4a)

$k_{p_i}^a$ pore diffusion mass transfer coefficient for Compartment i, Eq. (12a)

$k^a_{s_i}$	surface diffusion mass transfer coefficient for Component *i*, Eq. (12b)
L_m	length of mass transfer zone
m	Langmuir saturation adsorption capacity, Eq. (1)
n_i	amount of Component *i* adsorbed
$\bar{n}_i$	amount of Component *i* adsorbed in equilibrium with *P*, *T*, y_i
$\hat{n}_i$	amount of pure Component *i* adsorbed at *P* and *T*
$\tilde{N}_i$	average rate of adsorption of Component *i* in constant pattern mass transfer zone
P	gas pressure
Q	gas flow rate based on empty column cross section
q_i	isosteric heat of adsorption of Component *i*, Eq. (2)
R	gas constant
Re	Reynolds number = Qdp/μ
Sc	Schmidt number = $\mu RT/Dp$
T	temperature
t	time
y_i	mole fraction of Component *i* in gas phase at *z* and *t*
$\bar{y}_i$	mole fraction of Component *i* in equilibrium with *P*, *T*, and n_i
z	distance in column

Greek Letters

α	$(1 + \tilde{N}_2/\tilde{N}_1)$
β	velocity of front transfer zone
ε	external void fraction in column = 0.43
ε_l	pellet void fraction of large macropores in adsorbent
ε_s	pellet void fraction of small macropores in adsorbent
ρ_b	adsorbent bulk density
ρ_p	adsorbent particle density
θ	$(T - T^0)$
Ψ_{s_i}	$0.894/(1 - 0.106A_i^{0.25})$
Ψ_{p_i}	$0.775/(1 - 0.225A_i^{0.40})$
Λ_i	$[(n_i^* - n_i^s)/(y_i^* - y_i^s)](\rho_b RT)/P$
$\tau_Z(y_i)$	time in which the concentration of front mass transfer zone changes from y_i to y_i^s

Superscripts

s	initial column conditions
*	middle equilibrium section for Type I column dynamics

° feed conditions
~ average conditions in front mass transfer zone

Subscripts

i Component i (= 1, 2)
f external film

REFERENCES

1. S. Sircar and A. L. Myers, *Chem. Eng. Sci., 28,* 489 (1973).
2. D. Valenzuela and A. L. Myers. *Sep. Purif. Methods, 13,* 153 (1984).
3. T. Vermeulen, G. Klein, and N. K. Hiester, "Adsorption and Ion Exchange," in *Chemical Engineers' Handbook* (R. H. Perry and C. H. Chilton, eds.), McGraw-Hill, New York, 1973, Chap. 16.
4. C. N. Satterfield, *Mass Transfer in Heterogeneous Catalysis,* MIT Press, Cambridge, Massachusetts, 1970.
5. N. Wakao and J. M. Smith, *Chem. Eng. Sci., 17,* 825 (1962).
6. J. P. Henry, R. S. Cunningham, and C. J. Geankoplis, *Ibid., 22,* 11 (1967).
7. E. R. Gilliland, R. F. Baddour, G. P. Perkinson, and K. J. Sladek, *Ind. Eng. Chem., Fundam., 13,* 95 (1974).
8. K. J. Sladek, E. R. Gilliland, and R. F. Baddour, *Ibid., 13,* 100 (1974).
9. W. J. Thomas and J. L. Lombardi, *Trans. Inst. Chem. Eng., 49,* 240 (1971).
10. J. W. Carter and H. Hussain, *Chem. Eng. Sci., 29,* 267 (1974).
11. K. Miura, H. Kurahashi, Y. Inokuchi, and K. Hashimoto, *J. Chem. Eng. (Jpn.), 12,* 281 (1979).
12. R. Kumar and S. Sircar, *Chem. Eng. Sci., 41,* 2215 (1986).
13. S. Sircar and R. Kumar, *Ind. Eng. Chem., Process Des. Dev., 22,* 271 (1983).
14. C. Y. Pan and D. Basmadjian, *Chem. Eng. Sci., 25,* 1563 (1970).
15. S. Sircar, R. Kumar, and K. J. Anselmo, *Ind. Eng. Chem., Process Des. Dev., 22,* 10 (1983).
16. T. H. Hsiung and G. Thodos, *J. Heat Mass Transfer, 20,* 331 (1977).

Received by editor February 19, 1986